

TECHNICAL UNIVERSITY OF DENMARK

Development and validation of a general test method for concentrating solar collector fields

Ingrid Overgaard s154669

Master of Science in Engineering of Sustainable Energy
Technical University of Denmark
July 25, 2021

Supervisor:

Weiqliang Kong
Senior Researcher at DTU Civil
Engineering

Co-supervisor:

Adam R. Jensen
PhD Student at DTU Civil Engineering

Development and validation of a general test method for concentrating solar collector fields

Report written by:

Ingrid Overgaard

Advisor:

Weiqliang Kong

Co-advisor:

Adam. R. Jensen

DTU Civil Engineering

Technical University of Denmark

2800 Kgs. Lyngby

Denmark

s154669@student.dtu.dk

Project period: 4. January - 25. July 2021

ECTS: 35

Education: M.Sc.

University: Technical University of Denmark

Field: Sustainable Energy Engineering

Class: Public

Edition: 1. edition

Copyrights: © Ingrid Overgaard, 2021

Abstract

The need for energy in the world is increasing, and at the same time, the request for green energy is higher than ever. The world needs sustainable energy production, with minimal emission of greenhouse gasses, and solar energy can be a part of the provider. In this thesis a mathematical model predicting the short term and long term thermal performance of two concentrating solar collector fields is being developed. One field is consisting of parabolic trough collectors, and the other of Fresnel lens collectors. The mathematical model is developed using quasi-dynamic testing. It is both developed and validated using data from the collector fields. The model is validated and can be used for predictions of the thermal performance for both collector fields. Though, is it also concluded that the model can be improved. A modified quasi-dynamic testing model is also tested for the parabolic trough collector field. This model shows promising results.

Acknowledgements

First I would like to thank DTU for providing amazing opportunities and giving me knowledge I will never take for granted.

I would like to give a special thanks to my supervisor, Weiqiang Kong, who has throughout this entire project been very helpful and quick to help me whenever I had a question. His engagement in this project has been amazing, leading to good meetings where many ideas were developed.

Thanks to my co-supervisor, Adam R. Jensen, for providing data and giving advice for the Fresnel lens collector field.

Thanks to my mother, Dorte Andersen, and my sisters, Hanne Overgaard and Benedikte Overgaard, for their amazing support through the writing of this thesis. A huge thanks to my boyfriend, Loke Rantzau Olsen, for his encouragement and patience.

Finally, a special thanks to my father, who helped me through my first years at DTU, but unfortunately will not see me graduate. He always supported me in my academic steps, giving me courage and advice to fulfil my goals.

Without all of these people the completion of this thesis would not have been possible.

Contents

1	Introduction	1
1.1	Concentrating solar collectors	2
1.2	CSP fields investigated for this thesis	3
1.3	Thesis outline	4
1.4	Thesis overview	4
2	Literature review	5
2.1	Reports	5
2.2	Elaboration from earlier papers	6
3	Theory	7
3.1	Quasi-dynamic testing	7
3.2	Parameters	9
3.3	Multiple linear regression	14
3.4	Boundary conditions for the test data	14
4	CSP fields setup	16
4.1	Brønderslev - Parabolic trough collector field	16
4.2	Lendemarke - Heliac Fresnel solar collector field	17
5	Program development and assumptions	19
5.1	Data processing	19
5.2	Optimization of code	22
5.3	Validation of model	23
6	Results from multiple linear regression	24
6.1	Brønderslev - Parabolic trough collector field	24
6.2	Lendemarke - Fresnel lens solar collector field	26

7	Model validation	29
7.1	Brønderslev - Parabolic trough collector field	29
7.2	Lendemarke - Fresnel lens solar collector field	34
8	Discussion and future work	37
9	Conclusion	40
	References	42
	Appendix A	45
	Appendix B	46

Chapter 1

Introduction

Goal number 7 from UN's 17 global goals [27] is "Affordable and clean energy", and target 7.2 sounds:

"By 2030, increase substantially the share of renewable energy in the global energy mix."

This describes the vision for this thesis, which is to ensure all energy productions is sustainable, leaving a minimal carbon footprint for the future.

The world is in constant movement and so is the need for energy. An increasing energy demand, but also awareness of the potential damage when acquiring it, leads to new ideas and potential. The harm related to emission of greenhouse gasses during energy production, has created a new goal for the energy market: extract energy from renewable energy sources. The nature of earth gives amazing opportunities – wind blowing, oceans in constant movement, and the sun emitting power directly to the earth. All are sources with power ready to be harvested. With the sun delivering the amount of energy needed for a year for the entire Earth in just 1 hour [13], solar energy is a part of the future energy market, with its almost unlimited resources.

Solar energy does not only give opportunities in the electricity market, but also in the heating market. Both markets are in need of sustainable solutions. Solar thermal collectors give a great opportunity to utilize the solar radiation directly for heat production, and the simplicity of the systems is beneficial when constructing it. With an efficiency for photovoltaic collectors around 22% [34] and an efficiency for solar thermal collectors around 70% [33], solar thermal collectors can contribute even more to a sustainable transition.

The demand for heating comes from both residences and industry. For residences the heat can be used for heating of houses and water, and industry is using heat in production. For industry higher temperatures are required than for residential. Solar heating systems can be of small scale, only used for one or a few residences, or be of large scale created as solar heating fields. Solar heating fields can even be used for producing electricity with the implementation of steam turbines in the system.

The world has limited resources. Politics, finance and priorities can sometimes limit the implementation of renewable energy in the energy systems. Therefore, the price and requirements for the new systems needs to be as accessible as possible. A solar heating collector is sold with certain specifications describing the efficiency, but when implementing the collector in a field the output might not be as expected. In the field losses can occur, leading to difference in the expected efficiency. This difference should be known to the investor, which leads to the mission of this thesis.

The mission of this thesis is to be able to give an accurate prediction of the thermal performance for two types of concentrating solar collector fields. In this thesis the aim will be reached by developing and validating a mathematical model describing solar energy fields.

1.1 Concentrating solar collectors

Solar thermal collectors exist in many different designs with different purposes, but the idea behind all the collectors is to use the solar radiation to heat a fluid, which will then be used in various different applications. Most common is the flat plate collector, which is used for residences and the evacuated tube collector, also mainly used for residences [33]. The flat plate collector is used for low temperatures at 30-75°C and the evacuated tube is used for medium temperatures of 50-150°C [23]. These temperatures make them suitable heating used for residences, and also for lower temperatures used in industry. Both collector types can utilize beam and diffuse radiation.

Another type of solar thermal collectors is concentrating solar power, CSP, collectors. These collectors can be constructed in different ways, but common for all of them is that the solar radiation is concentrated to a small surface or focus point, heating up a fluid and then utilizing this for heating. These collectors produce heat at a much higher temperature, which make them suitable for other purposes. For this thesis two types of concentrating solar collectors will be used: Parabolic trough collector, PTC, and Fresnel lens collector, FLC. Below in Figure 1.1 and Figure 1.2 the PTC and FLC can be seen, respectively.

The PTC is constructed with large mirrors shaped in a parabolic shape reflecting the solar radiation from a large surface to a receiver tube, which contains a heat transfer fluid. For the PTC collector investigated the receiver is made of a tube of stainless steel insulated by the use of vacuum within a layer of glass. The collector is a horizontal 1-axis tracking collector, which means it will follow the path of the sun during the day, with movement in 1 axis. This is very important for the efficiency of the collector and will ensure the solar radiation hits the collector at the most optimal angle possible, leading to as much solar radiation as possible hitting the receiver. The PTC mainly utilize beam radiation, meaning radiation that is not scattered due to e.g. the surroundings or clouds. Scattered radiation is diffuse radiation, which will have different unpredictable directions, and therefore the collector cannot adjust to the radiation. Usually, the main radiation will also be beam radiation.



Figure 1.1: A parabolic trough collector, evaluated in this thesis. [1]



Figure 1.2: A Fresnel lens collector, evaluated in this thesis. [5]

The temperature range for the PTC is higher than for e.g. the flat plate collector or evacuated tube collector. The maximum outlet temperature for the PTC investigated in this thesis, and shown in Figure 1.1 is 400°C . The high temperature makes it useable for electricity production, but the collectors can also be used for district heating or industry at lower temperatures. The collector is not suitable for single use, but will be used in larger fields with multiple collectors. The main advantages of the PTC are the ability to remain at the same efficiency even at large temperature, low heat losses, and multiple applications of the heat, while one of the disadvantages is high cost.

The Fresnel lens collector evaluated in this thesis is seen in Figure 1.2 above. The principle behind the collector, is that solar radiation is hitting a Fresnel glass lens, which focuses the radiation to a smaller focus point behind the lens, where is fluid is heated. The fluid will flow in well insulated and flexible pipes between the multiple focus points of the collector. The collector is 2-axis tracking, meaning the solar radiation in principle always will hit the collector directly and ensure an incidence angle of 0° . Like the PTC the FLC mainly work with beam radiation. The specific collector has a maximum outlet temperature of 400°C . The collector will be used in collector fields. The main advantage for the Fresnel lens collectors compared to PTC is a lower price, due to less expensive materials.

Different types of heat transfer fluids, HTF, can be used for the collectors, depending on the temperature range the collectors are operating at, and the use of the heat. For this thesis, a thermal oil, and a glycol-water mixture is used for HTF. The glycol-water mixture has a lower freezing point compared to water, which will be useful for collectors placed in environments with temperatures below 0°C . Thermal oils has a higher boiling temperature, which can be desired in some concentrating solar collector fields [31].

1.2 CSP fields investigated for this thesis

In this thesis two concentrating solar collector fields are investigated. One collector field is located in Brønderslev in Denmark and is consisting of the parabolic trough collectors. The other collector

field is located in Lendemarke in Denmark and is consisting of the Fresnel lens collectors. Both collector types are concentrating solar collectors, but are constructed using two different principles, and thereby it cannot be assumed that the results of the analysis will be similar.

1.3 Thesis outline

The purpose of this thesis is to develop a general mathematical model to evaluate the thermal performance of the two different types of concentrating solar collector fields in-situ. It should both predict the short term and long term performance in transient weather conditions. The model is based on the quasi-dynamic test method, and existing data from the fields will be used for the development. For the first system a thermal collector field with parabolic trough collectors is evaluated, and for the second system a field with Fresnel lens collectors is evaluated. The model will be validated with data from the collector fields. A program will be developed for each system, which will be used to find the mathematical model and do the validation.

1.4 Thesis overview

In each chapter of this thesis both solar collector fields will be described. In Chapter 2 a literature review will be presented, as well as the elaboration done in this thesis compared to earlier studies. In Chapter 3 the required theory and tools used for developing the mathematical model will be presented. In Chapter 4 the two solar collector fields will be described in detail. The data used for the development will be presented as well. In Chapter 5 the program development and assumptions are explained, including the idea behind the model validation. In chapter 6 the results from the model development for both systems will be shown. In chapter 7 the validation of the mathematical model is shown. In chapter 8 a discussion of the results is performed, and in Chapter 9 a conclusion is presented.

Chapter 2

Literature review

In this chapter a literature review will be performed. In the literature review, papers investigating the same problem as this thesis will be reviewed. It will also be discussed how this thesis will elaborate on earlier papers.

2.1 Reports

Three reports will be evaluated. Two reports will be concerning the parabolic trough collector field, and one article is about the Fresnel lens collector. First a report written in 2020 will be evaluated. The report investigates the same PTC collector field as in this thesis. Second a report also investigating the PTC field in Brønderslev will be evaluated, and lastly a report about the performance and testing of a single Fresnel lens collector. All reports are from the Technical university of Denmark.

Development and validation of a test method for parabolic trough solar collector fields in solar heating plants (Alexis Mihalitsis, 2020 [3]):

The report is investigating the same parabolic trough collector field in Brønderslev, as investigated in this thesis. In the report a test method for the PTC field is developed and validated. The test method is based on the quasi-dynamic test model. For the validation of the model the relative error between the predicted useful energy output from the model and the measured output was found to be 18-23%. The peak efficiency for the collector is found to be 58%.

Brønderslev Hybrid Solar Power Plant (Jensen, Furbo and Perers, 2020 [16]):

The report is evaluating the parabolic trough collector field in Brønderslev. It is investigated using quasi-dynamic testing and the standard IEC 62862-3-2:2018. A simulation of the collector field was done using the software TRNSYS.

Test of Heliac 3rd Gen. Solar Collector (Jensen, 2020 [14]):

The report investigates the thermal performance of a single Fresnel lens collector. The model is tested with quasi-dynamic testing. In the report the peak efficiency of the collector is found to be 60.2%.

2.2 Elaboration from earlier papers

In this thesis a mathematical model based on quasi-dynamic testing will be developed and validated for an entire collector field, and not just for a single collector. This have been done for a parabolic trough collector field before in (Mihalitsis, 2020 [3]), but in this thesis the performance will be improved, and also a new theory will be tested. For this theory a new term is added to the quasi-dynamic testing model. In (Jensen, Furbo and Perers, 2020 [16]) a quasi dynamic testing method is used to evaluate the PTC field in Brønderslev as well, but the QDT model is different from the one tested in this thesis. Also, the mathematical model in this thesis will be developed with a purpose to be used for two types of concentrating solar collector fields, which was not the case for (Mihalitsis, 2020 [3]) and (Jensen, Furbo and Perers, 2020 [16]). The two types of concentrating solar power collector fields is the parabolic trough collector field and also a Fresnel lens collector field. For both fields the model is validated. A QDT model for the Fresnel lens collector field has not yet been investigated in any published papers, only the model and performance of a single collector has been done in (Jensen, 2020 [14]).

Chapter 3

Theory

To develop the mathematical model for both of the concentrating solar power fields, some knowledge regarding existing in-situ test methods needs to be obtained. The model is based on quasi-dynamic testing, and knowing the idea and theory behind this is essential.

In this chapter the theory behind the development of the mathematical model will be described. First the quasi-dynamic test method is presented, and then how all the necessary input parameters are calculated. In the end the concept behind the multiple linear regression is explained, as well as the boundary conditions for the data used in the model development.

3.1 Quasi-dynamic testing

Through time multiple test methods for finding the thermal performance of solar thermal collectors have been used. These methods have been further developed as well. Two of these models for in-situ test has been verified, and is described in the standard ISO 9806:2017 [6]. One model can be used for steady-state testing, known as the steady-state testing model, and the other can be used in dynamic conditions, known as the quasi-dynamic testing, QDT, model.

The test methods are developed for single collector testing, but in this thesis the QDT method will be used for an entire collector field. When the QDT model is used for an entire collector field, losses related to the field will occur and extra factors needs to be implemented in the testing model. These will be described in further details later on in this thesis.

The steady-state testing model can be used in-situ, but when using the testing model many requirements for the data used are applied. Measured data can only be used if the incidence angle is less than 20° [22]. Besides this many other conditions must be fulfilled for the test to be valid e.g. a requirement for global irradiance, which cannot be less than $700 \frac{\text{W}}{\text{m}^2}$. The fraction of diffuse radiation must be below 30% of the global irradiance. These requirement leads to multiple days of testing, which does not even assure good enough data. The time perspective for the test is therefore unknown.

Another test option is the quasi-dynamic testing method, hence QDT method. The data requirement used for the testing is not as comprehensive and strict, as for the steady-state method. There is no requirement for the fraction of diffuse irradiance and incidence angle, and the required global irradiance should be within a large interval. The quasi-dynamic test method makes it possible to make in-situ test quicker, using more data. And the less requirements make it suitable for changing weather conditions. Below in Eq. 3.1 the equation for the QDT can be seen [6], [30].

$$Q = A_G \cdot [\eta_{0,b} \cdot K_b(\theta_L, \theta_T) \cdot G_b + \eta_{0,b} \cdot K_d \cdot G_d - a_1 \cdot (T_f - T_a) - a_2 \cdot (T_f - T_a) - a_3 \cdot u' \cdot (T_f - T_a) + a_4 \cdot (E_L - \sigma T_a^4) - a_5 \cdot \frac{dT_f}{dt} - a_6 \cdot u' \cdot G - a_7 \cdot u' \cdot (E_L - \sigma T_a^4) - a_8 \cdot (T_f - T_a)^4] \quad (3.1)$$

Where:

- Q is the useful power output, [W]
- A_G is the gross area of the collector field, [m²]
- $\eta_{0,b}$ is the peak collector efficiency for zero loss, [-]
- K_b is the incident angle modifier for beam irradiance, [-]
- θ_L is the longitudinal incidence angle, [°]
- θ_T is the transversal incidence angle, [°]
- G_b is the beam irradiance, $\left[\frac{\text{W}}{\text{m}^2}\right]$
- K_d is the incident angle modifier for diffuse irradiance, [-]
- G_d is the diffuse irradiance, $\left[\frac{\text{W}}{\text{m}^2}\right]$
- G is the hemispherical irradiance, $\left[\frac{\text{W}}{\text{m}^2}\right]$
- a_1 is the heat loss coefficient dependent on the ambient temperature, $\left[\frac{\text{W}}{\text{m}^2 \cdot \text{K}}\right]$
- a_2 is the heat loss coefficient dependent on the temperature of the solar collector, $\left[\frac{\text{W}}{\text{m}^2 \cdot \text{K}^2}\right]$
- a_3 is the heat loss coefficient dependent on the wind speed, $\left[\frac{\text{W}}{\text{m}^2 \cdot \text{K}^3}\right]$
- a_4 is the heat loss coefficient dependent on the sky temperature, [-]
- a_5 is the thermal capacity of the collector, $\left[\frac{\text{J}}{\text{m}^2 \cdot \text{K}}\right]$
- a_6 is the wind speed dependence for zero loss efficiency, $\left[\frac{\text{s}}{\text{m}}\right]$
- a_7 is the wind speed dependent heat loss coefficient for sky temperature, $\left[\frac{\text{W}}{\text{m}^2 \cdot \text{K}^4}\right]$
- a_8 , $\left[\frac{\text{W}}{\text{m}^2 \cdot \text{K}^4}\right]$
- T_f is the mean fluid temperature, [°C]
- T_a is the ambient temperature, [°C]
- E_L is the longwave irradiance ($\lambda > 3 \mu\text{m}$), $\left[\frac{\text{W}}{\text{m}^2}\right]$

- u is the wind speed, $\left[\frac{\text{m}}{\text{s}}\right]$
- $u' = u - 3$, $\left[\frac{\text{m}}{\text{s}}\right]$
- σ is Stefan-Boltzmann constant, $\left[\frac{\text{W}}{\text{m}^2 \cdot \text{K}^4}\right]$

The QDT model consists of variable data input collected from the solar collector field, and constants which describes the model.

The idea behind the testing method is to calculate the maximum possible power output, and then subtract losses which will affect the total output.

For the development of the mathematical model for the concentrating solar collector fields, the QDT model used will be as seen below in Eq. 3.2.

$$Q = \eta_0 \cdot K_b(\theta_i) \cdot G_b - a_1 \cdot (T_f - T_a) - a_2 \cdot (T_f - T_a)^2 - a_5 \cdot \frac{dT_f}{dt} \quad (3.2)$$

Where: θ_i is the incidence angle, $[\circ]$.

Since the collectors are concentrating solar collectors, the term including the diffuse irradiance will not have any significant influence on the power output, and therefore the term including G_d is removed. The receivers in the collectors both have small surface areas, the concentration ratio [18] of the collectors are high, and both types of pipes containing the heat transfer fluid are insulated, so the heat loss dependent on wind speed, will be so limited, that the terms including a_3 , a_6 , and a_7 will be removed, as well as the a_4 dependent on the sky temperature. The same reasons apply when removing a_8 , since the losses due to radiation also will be negligible.

3.2 Parameters

To perform the QDT and developing the mathematical model a variety of necessary input parameters needs to be calculated. The equations and explanations of these will be reviewed below. The calculated variables are depending on each other, and will be presented in the order they needs to be calculated.

Solar time, t_{solar}

Solar time, t_{solar} , is the time depending on the path of the sun. At 12:00pm solar time the sun will be at solar noon, meaning it will be at the highest position in the sky of the day. The solar time and the local standard time is often not equal, since local times is given for large areas for simplicity. Therefore the local standard time need to be corrected to follow the path of the sun. Solar time is used for calculation of angles related to the suns position. The solar time is used when calculating the hour angle, which will be presented in Eq. 3.6. Below in Eq. 3.3 the equation of the solar time can be seen [4],[8].

$$t_{solar} = \frac{4 \cdot (L_{standard} - L_{local}) + E}{60} + t_{standard} \quad (3.3)$$

$L_{standard}$ is the standard longitude, L_{local} is the local longitude, $t_{standard}$ is the local standard time, and E is the equation of time shown below in Eq. 3.4.

$$E = 229.2 \cdot (0.000075 + 0.001868 \cdot \cos(B) - 0.032077 \cdot \sin(B) - 0.014615 \cdot \cos(2 \cdot B) - 0.04089 \cdot \sin(2 \cdot B)) \quad (3.4)$$

Where,

$$B = (n - 1) \cdot \frac{360}{365} \quad (3.5)$$

n is the number of the day in the year.

Hour angle, ω

The hour angle, ω , describes the movement of the sun in relation to the time of the day. For every hour the sun will move 15° . It is necessary to know the hour angle, to find the zenith angle, which will be presented in Eq. 3.8. The equation for the hour angle is given below in Eq. 3.6 [8].

$$\omega = 15 \cdot (t_{solar} - 12) \quad (3.6)$$

ω is given in [degrees]. t_{solar} is solar time.

Declination, δ

When the Earth circles around the sun, a tilt of the Earth causes the changing seasons. This is due to a changing position of the sun in the sky, where the tilt is causing the position of the sun in the sky to vary through the year. The position of the sun, declination, is given in degrees and is seen in relation to the equator. The declination is used when finding the zenith angle in Eq. 3.8. The equation for declination, δ is given below in Eq. 3.7 [8].

$$\delta = 23.45 \cdot \sin\left(360 \cdot \frac{284 + n}{365}\right) \quad (3.7)$$

δ is given in [degrees]. n is the number of the day in the year.

Zenith angle, θ_z

The zenith angle, θ_z , is the angle between the actual position of the sun and the zenith of the sun. The zenith is where the sun is highest in the sky during a year. In Eq. 3.8 the equation to find the zenith angle is shown [8].

$$\theta_z = \arccos(\cos(\phi) \cdot \cos(\omega) \cdot \cos(\delta) + \sin(\phi) \cdot \sin(\delta)) \quad (3.8)$$

θ_z is given in [degrees]. ϕ is the latitude, ω is the hour angle, and δ is the declination.

Solar azimuth, γ_s

The solar azimuth, γ_s , is the horizontal angle between south and the position of the sun. Below in Eq. 3.9 the equation for calculating the solar azimuth [8] is shown.

$$\gamma_s = \text{sign}(\omega) \cdot \left| \arccos \cdot \left(\frac{\cos(\theta_z) \cdot \sin(\phi) - \sin(\delta)}{\sin(\theta_z) \cdot \cos(\phi)} \right) \right| \quad (3.9)$$

γ_s is given in [degrees]. ϕ is the latitude, ω is the hour angle, θ_z is the zenith angle, and δ is the declination. $\text{sign}(\omega)$ means that γ_s will have the same sign as ω .

The solar azimuth is used to find the incidence angle.

Incidence angle, θ_i

The incidence angle, θ_i describes at which angle the radiation from sun is hitting the collector surface. When the radiation is perpendicular to the surface the incidence angle will be 0° . Knowing θ_i is of great importance to be able to calculate the incidence angle modifier, the end effect loss and the shading coefficient for the collectors. The meaning of these will be described later. Below in Eq. 3.10, Eq. 3.11, and Eq. 3.12 the equations for finding the incidence angle for 1-axis horizontal tracking is presented [25].

If the collector is orientated as N-S tracking the θ_i would be as in Eq. 3.10 below.

$$\theta_{i,NS} = \arccos\left(\sqrt{1 - \cos^2(90 - \theta_z) \cdot \cos^2(\gamma_s)}\right) \quad (3.10)$$

θ_i is given in [degrees]. θ_z is the zenith angle, and γ_s is the solar azimuth.

If the collector is orientated as E-W tracking the θ_i would be as in Eq. 3.11 below.

$$\theta_{i,EW} = \arccos\left(\sqrt{1 - \cos^2(90 - \theta_z) \cdot \sin^2(\gamma_s)}\right) \quad (3.11)$$

If the collector is not tracking S-N or E-W, but the azimuth is deviating from this, θ_i is found as in Eq. 3.12.

$$\theta_{i,1axis} = \arccos\left(\sqrt{1 - \cos^2(90 - \theta_z) \cdot \cos^2(\gamma_s - \gamma)}\right) \quad (3.12)$$

γ is the azimuth of the collector.

If the collector is a 2-axis tracking collector, the incidence angle will theoretically always be 0° , if the collector is tracking perfectly. In this case the incidence angle is as below in Eq. 3.13:

$$\cos(\theta_{i,2axis}) = 1 \quad (3.13)$$

Incidence angle modifier, K_b

The incidence angle modifier, IAM, for beam radiation is represented by the variable K_b . K_b is a value usually between 0 and 1, describing how much of the solar radiance hitting the collector is actually used. IAM is dependent on the incidence angle - the lower the incidence angle, the higher K_b , resulting in high power for the system. K_b can exceed 1 if e.g. reflection on to the collector occur [24]. Below in Eq. 3.14 the equation for the IAM [10] is shown.

$$K_b(\theta_i) = \cos(\theta_i) + b_1 \cdot \theta_i + b_2 \cdot \theta_i^2 \quad (3.14)$$

b_1 and b_2 are constants describing the IAM, and θ_i is the incidence angle.

For a 2-axis tracking collector, with assumed perfect tracking the incidence angle is assumed to be 0° at all time. Therefore the IAM will be as in Eq. 3.15 below.

$$K_{b,2axis} = 1 \quad (3.15)$$

Shade coefficient, η_{shade}

When the collectors are placed in front of each other in the collector field, a loss from shading will occur even though there is a certain distance between each row. The loss will be significant in the early morning and late afternoon when the sun is low in the sky. A shade coefficient, S , can be calculated as below in Eq. 3.16 [29].

$$S = |\cos(\rho)| \cdot \frac{d_{row}}{w_{coll}} \quad (3.16)$$

Where d_{row} is the distance between each row, w_{coll} is the width of the collectors, and ρ is the tracking angle for the collector found as below in Eq. 3.17 [25].

$$\rho = \arctan\left(\frac{\sin(\gamma_s - \gamma)}{\tan(90 - \theta_z)}\right) \quad (3.17)$$

γ_s is the solar azimuth angle, γ is the azimuth angle of the collectors, and θ_z is the zenith angle.

The tracking angle is shown in Figure 3.1 below. It is the angle between a line perpendicular to the surface of the earth and a line perpendicular to the collector surface.

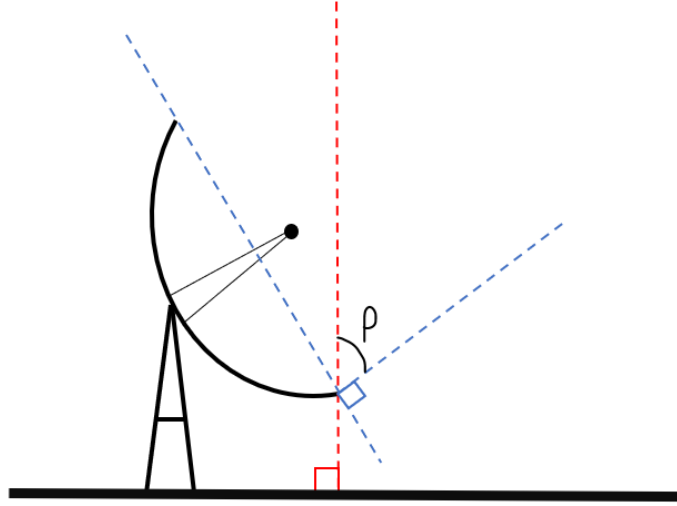


Figure 3.1: Tracking angle, ρ , for 1-axis tracking parabolic trough collector.

Not all collectors will be shaded during the day. Those collectors, unshaded collectors, are placed at the first row in the collector field. Below in Eq. 3.18 the expression of the actual shading coefficient for the entire field is shown.

$$\eta_{shade} = \frac{n_{collector} - n_{unshaded}}{n_{collectors}} \cdot S + \frac{n_{unshaded}}{n_{collectors}} \quad (3.18)$$

Where S is the shade coefficient found in Eq. 3.16, $n_{collector}$ is the total number of collectors, and $n_{unshaded}$ is the number of unshaded collectors in the field.

End-loss effect, η_{end}

End-loss effect will only be present for the PTC. It is a coefficient describing how much of the energy reflected in the mirrors of the PTC, that will be reaching the receiver [18]. If the solar radiation is not hitting the collector perfectly perpendicular, the angular difference, will results in some beams will not be reflected towards the receiver tube. In Eq. 3.19 the equation for end-loss effect, η_{end} , is shown [20].

$$\eta_{end} = 1 - \frac{(1 + \frac{w_{coll}^2}{48 \cdot f^2}) \cdot \tan(\theta_i)}{l_{coll}} \quad (3.19)$$

w_{coll} is the width of the collector, f is the focal length of the collector, θ_i is the incidence angle, and l_{coll} is the length of the collector.

Calculated power output, q_u

When developing the mathematical model a power output value for the system, q_u , needs to be calculated. q_u is the useful power output for each time step in the model. This is used as a value

for Q in the QDT model, so it is possible to estimate the remaining constants in the model. The equation for the calculated power output can be seen below in Eq. 3.20 [8].

$$q_u = \dot{m} \cdot C_p \cdot (T_o - T_i) \quad (3.20)$$

q_u is in [W]. \dot{m} is the mass flow rate, C_p is the specific heat capacity, T_o is the outlet temperature of the fluid, and T_i is the inlet temperature of the fluid.

q_u is calculated for the heat transfer fluid, HTF, in the collector, but can also be applied for the secondary side of the heat exchanger, HX. This can be used in cases, where q_u for the primary side of the heat exchanger cannot be calculated easily and accurate. If the efficiency of the HX is low, it should be taken into account. In those cases q_u should be divided with the efficiency of the HX, in order to get the correct power output from only the collectors.

3.3 Multiple linear regression

The unknown constants from the QDT model are found with a multiple linear regression, MLR. This regression is used to estimate constants for each term in a equation, to describe the slope of the regression, using a known output and variable inputs. Below in Eq. 3.21 the general expression for the MLR can be seen [28].

$$y_i = \beta_0 + \beta_1 \cdot x_{i1} + \beta_2 \cdot x_{i2} + \dots + \beta_p \cdot x_{ip} + \epsilon \quad (3.21)$$

For the QDT model, varying data from the collector field describing the weather condition is used as the input. These inputs will be as x_{ip} in Eq. 3.21. The expected output is calculated as in Eq. 3.20, and will be y in Eq. 3.21. The fitted constants will be as β_p in Eq. 3.21. The fitted constants from the regression will then describe the constants desired to know from the QDT model.

3.4 Boundary conditions for the test data

The mathematical model is developed using actual measured data at the collector fields, which can be difficult to use, if it is not treated correctly. To develop an mathematical model as accurate as possible, a set of boundary conditions, is applied for the test data, when used in the model development with QDT. These boundaries conditions define the requirements for the data used in the model development.

For the PTC field these conditions ensure, that only data from online collectors are used, and that data from e.g. night will be removed, as well as data errors. The same conditions will apply for the FLC field, except for the second condition seen below in Table 3.1. This a due to a lack of data, so the required knowledge cannot be obtained to fulfil the conditions. Below in Table 3.1 the boundary conditions for the PTC field can be seen.

Parameter condition	Unit
$G_b \geq q_u$	$\frac{W}{m^2}$
Percent online collectors > 0	%
$q_u \geq 100$	$\frac{W}{m^2}$
$G_b \geq 100$	$\frac{W}{m^2}$
$-0.01 < \frac{dT_f}{dt} < 0.01$	$\frac{^\circ C}{min}$

Table 3.1: The boundary conditions for the PTC field test data used in the development of the mathematical model.

$G_b \geq q_u$:

The energy output should never be higher than the irradiance level. The collector field cannot produce more energy than is delivered to the collectors. If the condition is not fulfilled, it would mean there is an error in the data, and therefore the data from the timestamp has to be removed.

Percent online collectors > 0:

When no collectors are online, meaning they will not track the sun correctly, there will be no energy output even though the irradiance is high. The data will therefore be removed, so it does not affect the constants found from the MLR. For the calculations this condition is only used for the PTC field, but it could also be used for the Fresnel collector field, if the data is available.

$G_b \geq 100$ and $q_u \geq 100$:

If the irradiance or energy output is too low, it will cause errors when finding the MLR, so some requirements have to be set. In this thesis they are chosen to be at least $100 \frac{W}{m^2}$.

$-0.01 < \frac{dT_f}{dt} < 0.01$:

Large changes in the mean fluid temperature, T_f , in short time will affect the MLR. T_f changes all the time, but to limit deviations for the model development a limit for the fluctuations is necessary.

Chapter 4

CSP fields setup

In this chapter the two systems with the Parabolic trough collectors and Fresnel lens collector will be presented. The knowledge about the fields is very important to successfully create the mathematical model.

4.1 Brønderslev - Parabolic trough collector field

The Parabolic trough collector field, PTC field, is placed in Brønderslev, Northern Jutland in Denmark. The field is owned by Brønderslev Forsyning, and established by Aalborg CSP. It has a capacity of 16.6 MW, and started operation at the end of 2016. It is placed at latitude 57.27°N and longitude 9.94°E .

The collectors are all placed in the same direction facing 29.9° E of North, and are 1-axis horizontal tracking collectors. The collector field is consisting of 40 rows of 10 collectors each, so 400 collectors in total. Each of the 400 collectors has a width of 5.77 m and length of 12 m. The total aperture area of the entire collector field is 26930 m^2 and the maximum optical efficiency claimed by the producer is 77%. 27 out of the 400 collectors are assumed not be shaded during the day, since no collectors are placed in front of them. Below in Figure 4.1 the placement of the collectors in the field can be seen.

For the model development and validation data from the PTC field is used. The data is from May 2017 to September 2017, and has a time resolution of 1 min between each data step, meaning the data will be saved every 1 minute. The time-series are given in daylight-savings time, which will be corrected in the program. The data files contain all information, including temperature differences, beam irradiance, flow rate, and tracking angles of each of the collector rows.



Figure 4.1: Parabolic trough collector solar field in Brønderslev. [11]

The heat transfer fluid, HTF, used in the collectors is a thermal oil "Therminol 66". The fluid properties - density and specific heat capacity - is provided in a data file, and is used for the model development.

The collectors are not always tracking correct and will in those cases not deliver the maximum energy output. This can e.g., be caused by fault in the tracking system or purposely defocusing of the collectors, due to too high temperatures. To limit errors when developing the mathematical model, this needs to be accounted for in the model. When a collector is tracking correct, it will be stated as online. To find the online collectors, a difference between the optimal angle of the collector and the actual angle, cannot exceed 2° . The 10 collectors combined in one row will all have the same angle. In Eq. 5.5 in Chapter 5 this will be described further.

4.2 Lendemarke - Heliac Fresnel solar collector field

The Heliac Fresnel solar collector field is placed in Lendemarke, Møn, Denmark. The solar collectors are from the Danish company Heliac, who in collaboration with the company E.ON has created the collector field. The specific location of the field is at latitude 54.979°N and longitude 12.267°E . Below in Figure 4.2 the collector field can be seen.

The collector field is constructed with 144 collectors. Each collector is created with 8 Fresnel lenses and has an aperture area of 16.55m^2 . The collector is a 2-axis tracking collector, making sure the radiation from the sun will always hit directly perpendicular at the collector. The capacity of

each panel is 12 kW [12]. The heat transfer fluid used for the collectors is 30% glycol and 70% water mixture.



Figure 4.2: Heliostatic Fresnel solar collector field in Lendemarke. [9]

One day of data is available from the collector field. The data is from 22nd of September 2020, and the data has a time resolution of 1 minute. Approximate $2/3$ of the collectors were online when the data was measured. The local time is given in daylight-savings time. Only one day of data will limit the accuracy when developing the mathematical model and performing the validation. This will be described further in Chapter 5.

Chapter 5

Program development and assumptions

In order to write the program, a walk-through of the fundamental program knowledge and assumptions is necessary.

In this chapter the idea behind the program development for both model development and validation will be presented. The programming platform used for program development will be presented, as well as the equation used for the MLR and the assumptions for averaging values for each time step.

5.1 Data processing

To find the parameters from the MLR a program for each collector field is written in MATLAB. In this chapter the main calculations done in the code and the assumptions will be presented.

MATLAB version R2020a is used as the solving tool for the MLR and for the validation. MATLAB is chosen due to the programs many possibilities when working with large data sets, as well as the graphical possibilities when plotting graphs.

Model development - For PTC field

The developing of the mathematical model for the PTC field will be based on the QDT model presented in Eq. 3.2. It will be derived as below in Eq. 5.1 and Eq. 5.2, when inserting the equation for K_b presented in Eq. 3.14.

$$Q_{PTC,modified} = \eta_0 \cdot (\cos(\theta_i) + b_1 \cdot \theta_i + b_2 \cdot \theta_i) \cdot G_b \cdot \eta_{shade} \cdot \eta_{end} - a_1 \cdot (T_f - T_a) - a_2 \cdot (T_f - T_a)^2 - a_5 \cdot \frac{dT_f}{dt} \quad (5.1)$$

$$\Rightarrow Q_{PTC,modified} = \eta_0 \cdot G_b \cdot \eta_{shade} \cdot \eta_{end} \cdot \cos(\theta_i) - \eta_0 \cdot G_b \cdot \eta_{shade} \cdot \eta_{end} \cdot b_1 \cdot \theta_i - \eta_0 \cdot G_b \cdot \eta_{shade} \cdot \eta_{end} \cdot b_2 \cdot \theta_i^2 - a_1 \cdot (T_f - T_a) - a_2 \cdot (T_f - T_a)^2 - a_5 \cdot \frac{dT_f}{dt} \quad (5.2)$$

Where:

- η_{shade} is the shading coefficient, [-]
- η_{end} is the end-loss effect, [-]

In Eq. 5.1 and Eq. 5.2 the shading coefficient, η_{shade} , and the end-effect loss, η_{end} , are included. These were found in Eq. 3.16 and Eq. 3.19 above in Chapter 3 - Theory.

From Eq. 5.2 it can be seen, that the QDT model contains six terms, and the unknown constants are: η_0 , b_1 , b_2 , a_1 , a_2 , and a_5 . These are the constants desired to find with the MLR.

The known variables in Eq. 5.2 are G_b , θ_i , η_{shade} , η_{end} , T_f , and T_a . These will be calculated as presented in Chapter 3 - Theory. Some of the calculations from Chapter 3, will be altered before used in the calculations for the PTC field. This is to adjust them to the actual operation of the field, which i.a. include fraction of online collectors. The adjusted equations will be presented in this section.

The mean fluid temperature, T_f is found as the mean values between the inlet temperature of the collector, $T_{in,HTF}$, and outlet temperature of the collector, $T_{out,HTF}$, as shown below in Eq. 5.3.

$$T_f = \frac{T_{in,HTF} + T_{out,HTF}}{2} \quad (5.3)$$

Q from Eq. 5.2 is the calculated q_u for the secondary side of the HX. q_u is found for the secondary side of the HX, since it could not be calculated accurately on the primary side of the HX. The calculation of q_u is shown below in Eq. 5.4. q_u from 3.20 is divided with the area of the collectors times the fraction of online collectors to get the output in $\left[\frac{W}{m^2}\right]$.

$$q_u = \frac{m_{water} \cdot C_{p,water} \cdot (T_{o,water} - T_{i,water})}{A_{total} \cdot \eta_{online}} \quad (5.4)$$

A_{total} is the total aperture area of the collector field. η_{online} is the fraction of online collectors, found as described below in Eq. 5.5 and Eq. 5.6.

$$\eta_{online,collector} = \begin{cases} 1, & \text{if } \Delta a_{diff} \leq 2^\circ \\ 0, & \text{if } \Delta a_{diff} > 2^\circ \end{cases} \quad (5.5)$$

Δa_{diff} = "Actual angle of collector" - "Best angle of collector"

The sum of the rows for each time step is found and divided with the number of rows, to find the fraction of online collectors for each time step.

$$\eta_{online} = \frac{\sum \eta_{online,collector}(t)}{N_{rows}} \quad (5.6)$$

When developing the model approximately one month of data from the collector field is used as input for the MLR. For the PTC field the data from May 3rd 2017 to May 31st 2017 is used.

The mathematical model derived in Eq. 5.2, will be compared to the same model, but including a new term a_3 . The model and procedure for the MLR will be the identical, except that the term $a_3 \cdot (T_f - T_a)^3$ will be included. The derived model with the a_3 term can be seen below in Eq. 5.7. This model will be denoted as $Q_{PTC,modified}$.

$$Q_{PTC,modified} = \eta_0 \cdot K_b(\theta_i) \cdot G_b \cdot \eta_{shade} \cdot \eta_{end} - a_1 \cdot (T_f - T_a) - a_2 \cdot (T_f - T_a)^2 - a_3 \cdot (T_f - T_a)^3 - a_5 \cdot \frac{dT_f}{dt} \quad (5.7)$$

Derived the equation will be as in Eq. 5.8 below.

$$Q_{PTC,modified} = \eta_0 \cdot G_b \cdot \eta_{shade} \cdot \eta_{end} \cdot \cos(\theta_i) - \eta_0 \cdot G_b \cdot \eta_{shade} \cdot \eta_{end} \cdot b_1 \cdot \theta - \eta_0 \cdot G_b \cdot \eta_{shade} \cdot \eta_{end} \cdot b_2 \cdot \theta^2 - a_1 \cdot (T_f - T_a) - a_2 \cdot (T_f - T_a)^2 - a_3 \cdot (T_f - T_a)^3 - a_5 \cdot \frac{dT_f}{dt} \quad (5.8)$$

For a_3 included in Eq. 5.7, the wind speed, u , is not included, as for a_3 in Eq. 3.1. The new term $a_3 \cdot (T_f - T_a)^3$ tested and evaluated specifically for this thesis. It is desired to know if the extra heat loss term has an effect on the performance of the QDT model. The reason for adding the new term is that the heat loss from the collector, might be more complicated, than it is possible to describe with a second-degree polynomial. Therefore a higher order polynomial - third-degree polynomial - is tested. When testing this idea it is compared to the measured useful output for validation.

The reason for testing both the model in Eq. 5.2 and Eq. 5.7 is to compare the results, and see if the added term for heat loss, improves the results. Also the model without a_3 is evaluated to see, if the QDT model can be used for the PTC field.

Model development - For Fresnel lens collector field

The collectors in the Fresnel lens collector field are 2-axis tracking collectors, which are assumed to be perfectly tracking. This will mean, that the collectors always receive the solar radiation perpendicular to the surface of the collector. Therefore the incidence will be 0° at all time, and the IAM, K_b , will be 1.

The QDT model shown in Eq. 3.2 will be evaluated for the Fresnel lens collector field, but with some alterations. The QDT model including the new term a_3 presented in Eq. 5.7 will not be evaluated,


the reason for this will be explained in Chapter 6 - Results from multiple linear regression. Below in Eq. 5.9 the QDT model of the FLC field can be seen.

$$Q_{FLC} = \eta_0 \cdot G_b - a_1 \cdot (T_f - T_a) - a_2 \cdot (T_f - T_a)^2 - a_5 \cdot \frac{dT_f}{dt} \quad (5.9)$$

The QDT model for the FLC field will have small changes due to the construction of the collector. Since K_b is 1 the term will not affect the model, and will be removed. The end-effect, which was including the mathematical model for the PTC field, is not present at the FLC. A shading coefficient is not calculated for the field, as the geometric data was not available, and therefore this is not included in the model.

For the FLC field the measured useful energy output, q_u , is found using a measured power output, $Q_{measured,FLC}$, in [kW] on the primary side of the heat exchanger. It is desired to have the power in the unit $\left[\frac{W}{m^2}\right]$, so recalculations need to be done, as seen below in Eq. 5.10.

$$q_u = \frac{Q_{measured,FLC} \cdot 10^3}{A_{total} \cdot \frac{2}{3}} \quad (5.10)$$

q_u is measured useful power output for the FLC field in $\left[\frac{W}{m^2}\right]$, A_{total} is the total aperture area of the collector field. The area is multiplied with $\frac{2}{3}$, since that is the fraction of online collectors in the time period of the measurement. 

The mean fluid temperature is again found as the mean of the inlet and outlet temperature of the collectors, as shown in Eq. 5.3. The direct normal irradiance, DNI, is used as G_b from Eq. 5.9, since the collector is tracking in 2-axes.

5.2 Optimization of code

In Appendix A a flowchart for the coding of the mathematical model for the solar collector fields can be seen. The flowchart is showing in which order the calculations of the variables is done, as well as the programming structure in general. In Appendix B a flowchart of the code written to calculate the predicted useful power output is shown. The flow charts are showing the programming structure for PTC field, but the same programming flow will apply for the FLC field, though with another procedure for implementation of the incidence angle and IAM in the QDT model.

When performing the calculations of the variables for the QDT model the time resolution of the output is determined by the time resolution of the given data. The time resolution is how much time, there is between each measured data point. The measured data for both the PTC field and the FLC field has a time resolution of 1 minute. Though, when finding the MLR constants it is desired to use data of larger time steps, to limit the large fluctuations which can be present in the measured data. The fluctuation can be due to sudden weather changes e.g. bypassing clouds affecting the received irradiance. The measured data shows reality, which includes the quick deviations in beam irradiance, when the weather is changing. Even though, the MLR can still be used for smaller time steps, the deviations will result in a less precise model.

A resolution of both 5 and 10 minutes was tested, but the best results were achieved at 5 minute time steps. This was also the conclusion from (Fahr, Tschopp, Nielsen, Kramer, and Ohnewein, 2020 [26]), where a 5 minute resolution for in-situ testing was found to give the most valid results. If the time steps are too large, it will result in errors in the derived constants from the MLR, since the variable data will not sufficiently describe the weather conditions. The larger time resolution of 5 minutes will also make it quicker to run the model.

5.3 Validation of model

To ensure the mathematical model is acceptable for describing the collector field, it has to be validated. When the model is validated the useful output predicted with the mathematical model is compared to the actual measured useful output, both for the same time period. If there is no large difference between the values, the model can be assumed to be valid.

For the validation the collector data is used as an input to the mathematical model, and thereby the energy output, Q , can be calculated. This output will be considered as the "predicted energy output". The predicted output can then be compared to the actual energy output for the time period, which is the "measured energy output".

When the mathematical model is validated, data from the collector fields is used. Multiple months of data would be preferred, to ensure the most valid results of the validation. For the PTC field data from June, July, August and September 2017 is used. For the FLC field only data from the 22nd of September 2020 is available. This will affect the validation, since both the model development and validation are performed using the same data set. Also, with the limited data, the performance of the mathematical model under changing weather conditions can be difficult to validate.

For the validation, data with large unrealistic deviations, will be removed in a data filter. These deviations will not be scientifically possible, and therefore they are designated as data errors. Removing this data will ensure the power output will not be affected by data errors.

Chapter 6

Results from multiple linear regression

In this chapter the results from the MLR will be presented. The results are the constants from the QDT model. The constants will describe important factors about the collectors. The impact of shading and end-loss effect for the parabolic trough collector will also be presented.

6.1 Brønderslev - Parabolic trough collector field

The input parameters to the MLR are calculated as shown in Chapter 3. Below in Figure 6.1 the shading coefficient can be seen and Figure 6.2 shows the end-loss effect for over a day. Both figures are displaying the variables from the 17th of May 2017.

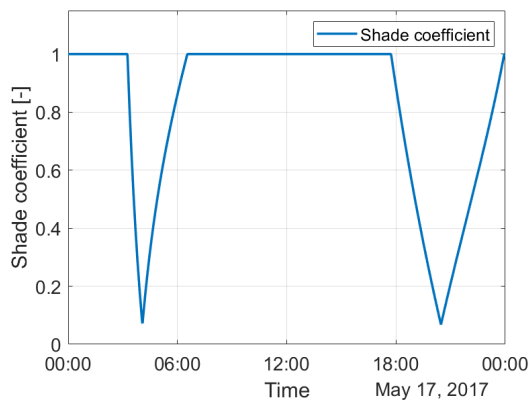


Figure 6.1: Shading coefficient for the PTC field seen for one day - 17th of May 2017.

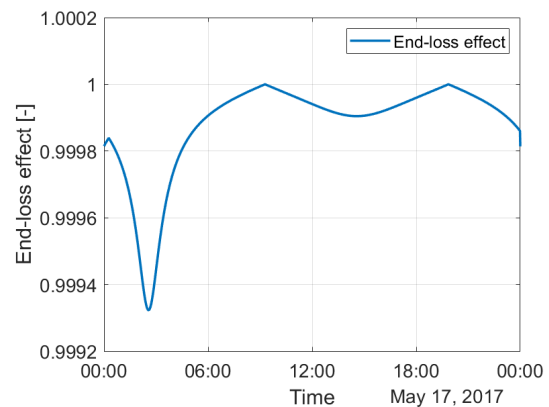


Figure 6.2: End-loss effect for the PTC field seen for a day - 17th of May 2017.

From Figure 6.1 it can be seen, that the shading coefficient is 1 for most of the day, where there

will be no shading affecting the panels. The coefficient is lower in early morning and evening as expected. The sun will be low in the sky at these times, and therefore some panels will be more affected by shading from the other collector rows.

Looking at Figure 6.2 it can be concluded that the end-loss effect is very low. The biggest effect is seen in early morning, as for the shading coefficient. With the biggest impact from end-loss effect being approximate 0.0006% it will have almost no effect on the collector performance.

As described in Chapter 3 - Section 3.3 - MLR is used to find the constants from the QDT models shown in Eq. 5.2 and Eq. 5.8. These have been found to be the values in Table 6.1. In Table 6.1 the values found in the earlier study (Mihalitsis, 2020 [3]) are also presented. These values will be used for comparison.

	η_0	b_1	b_2	a_1	a_2	a_3	a_5
<i>Unit</i>	-	-	-	$\frac{W}{m^2 \cdot K}$	$\frac{W}{m^2 \cdot K^2}$	$\frac{W}{m^2 \cdot K^3}$	$\frac{J}{m^2 \cdot K}$
Constants from QDT model without a_3 term	0.5998	-0.0018	$2.235 \cdot 10^{-6}$	-1.3829	0.0189	-	-3949
Constants from QDT model with a_3 term	0.6132	-0.0035	$2.379 \cdot 10^{-5}$	-4.9236	0.0807	$-2.63 \cdot 10^{-4}$	-3916
<i>QDT constants found from (Mihalitsis, 2020 [3])</i>	0.58	0.0047	$-1.4 \cdot 10^{-4}$	-0.7	0.01	-	-3163

Table 6.1: Table showing the constants from the QDT models.

η_0 describing the peak efficiency of the collector is 59.98% for the model without a_3 , and 61.32% for the model including a_3 . A small increase can be seen in the modified model including a_3 . These peak efficiencies are higher, than found in (Mihalitsis, 2020 [3]). The heat loss, a_1 , and thermal capacity, a_5 , is in this thesis higher, than the values found in (Mihalitsis, 2020 [3]). The values found in (Mihalitsis, 2020 [3]) were also found for the entire collector field. For a collector field a_1 and a_5 will be higher than for a single collector, since the constants now describe an entire collector field, which includes piping. b_1 and b_2 describing the IAM are varying for the two models, but even though when finding $K_b(\theta_i)$ the curves are very similar. In Figure 6.3 the IAM for the two models can be seen for one day - the 17th of June 2017.

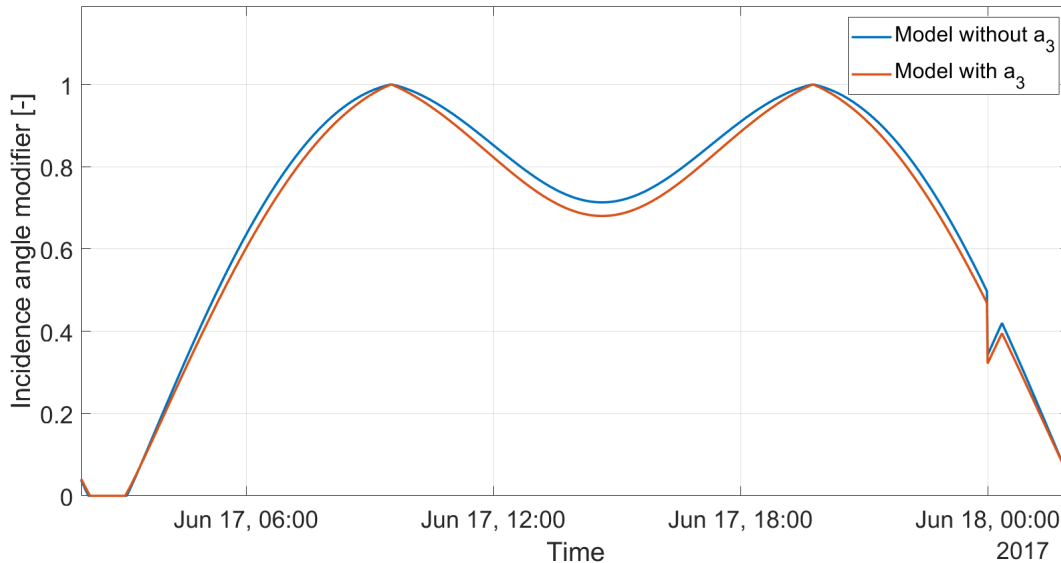



Figure 6.3: Incidence angle modifier on the 17th of June 2017: The QDT model without a_3 (blue curve) and QDT model with a_3 (orange curve). The x-axis is showing the local time.

The heat loss a_2 is found to be positive, which does not indicate a heat loss. Nevertheless, the common loss from the a_1 term and a_2 term is still negative, resulting in a heat loss. The heat loss coefficients a_1 and a_2 is much higher for the modified model. The extra heat loss coefficient a_3 is not high, but even though it could be the case, that a more detailed description of the heat loss will be more applicable when comparing the measured and predicted useful output. This will be further investigated in the model validation in Chapter 7.

The coefficient of determination, R^2 , is for the model without a_3 $R^2 = 0.929$, and for the model with a_3 $R^2 = 0.932$. This means that the model including a_3 will fit the data better. Higher R^2 -values would be desired, but considering the data is measured in-situ under dynamic conditions, the values are acceptable.

6.2 Lendemarke - Fresnel lens solar collector field

The constants in Eq. 5.7 is found. The values for these can be seen below in Table 6.2. The table also shows QDT constants found from a single FLC found from (Jensen, 2020 [14]). The QDT model for the single collector from (Jensen, 2020 [14]) consist of other terms, diffuse IAM and a_3 , but even though can the constants still be compared.

	η_0	K_d	a_1	a_2	a_3^*	a_5
<i>Unit</i>	-	-	$\frac{W}{m^2 \cdot K}$	$\frac{W}{m^2 \cdot K^2}$	$\frac{J}{m^3 \cdot K}$	$\frac{J}{m^2 \cdot K^2}$
QDT constants from model 	0.61	-	-13.1	0.24	-	-4618
<i>QDT constants found from (Jensen, 2020 [14])**</i>	0.602	0.02	-0.23	-	-0.178	-3357

*The a_3 term used in (Jensen, 2020 [14]) is dependent on the wind speed as shown in Eq. 3.1: $a_3 \cdot (T_f - T_a)$. a_3 in this table cannot be compared with a_3 found in Table 6.1.

** The constants found are for a single Heliac Fresnel lens collector.

Table 6.2: Constants found for the QDT model. The constants from (Jensen, 2020 [14]) are also presented. These are for at single Fresnel lens collector.

For the model in Eq. 5.7 is $R^2 = 0.92$, so the fit is acceptable, but an increase in R^2 could be desired. This value is close to the R^2 -values found from the PTC field.

Looking at the constants from the QDT model seen in Table 6.2, the first constant to notice is the very high heat loss a_1 of $-13.1 \frac{W}{m^2 \cdot K}$. It is much higher than what would be expected, also compared to the value for the single collector, where a_1 was found to be $-0.23 \frac{W}{m^2 \cdot K}$. Even though the value for the found constant is too high, it still shows the tendency, that would be expected, when finding the heat loss for the entire collector field. The heat loss a_1 for the entire field, is not just describing the heat loss from the collector, but also for the pipes transporting the HTF. These pipes are not only transporting the heat between each of the collectors, but also from the collector field to a heat exchanger. Therefore the heat loss is larger for the entire field, than for a single collector.

Another reason for a high a_1 heat loss, might be a missing integration of the heat loss dependent on the wind speed. For the single collector analysis in (Jensen, 2020 [14]) a heat loss dependent on wind speed was found to be $-0.178 \frac{J}{m^3 \cdot K}$. The heat loss dependent on wind speed was not implemented in the QDT model for the collector field, due to missing data. This will mean that a potential wind speed dependent heat loss will be represented in the a_1 heat loss as well.

Another constant to notice is the heat loss a_2 .  The constant is positive, which would not be expected for a heat loss. This might indicate that the term is not significant for the model.

The peak efficiency, η_0 for the collector, found to be 61%, seems very reasonable. The thermal capacity of the collector field, a_5 is found to be $4618 \frac{J}{m^2 \cdot K^2}$, which is higher than the thermal capacity found for a single collector. It is higher because the thermal capacity is found for the the entire collector field, which also includes the piping.

The QDT model including the a_3 term, as was investigated for the PTC field, is not investigated for the FLC field. The very limited data resulted in invalid and wrong values for the constants.

The limited data has properly affected the constants found for the FLC field, but still the results can give an useful estimate of the constants in the QDT model.

Chapter 7

Model validation

In this chapter the validation of the mathematical model for the PTC field and the Fresnel lens collector field will be performed. The validation will make it possible to see, if the model is fitting the measured data as desired, and is thereby valid. A comparison of the daily measured and predicted power output will be done, as well as the monthly energy output. The daily power output comparison will show the performance of the model for short term predictions, whereas the monthly comparison will show the long term performance of the model.

The validation of the mathematical model for the PTC field, will be compared with validation of a model from another report.

7.1 Brønderslev - Parabolic trough collector field

The parameters from Table 6.1 are inserted in Eq. 5.2 and Eq. 5.8, and the useful power output is found for June, July, August and September 2017.

Below in Figure 7.1 and 7.2 a graphical representation of the measured power output, the predicted power output Q_{PTC} from the QDT model without a_3 , and the predicted power output, $Q_{PTC,modified}$, from the QDT model with a_3 is shown in $\frac{W}{m^2}$. Notice the different scaling on the y-axes. Figure 7.1 shows the power output from the 13th of June 2017. It was a sunny day with limited cloud cover, which can be seen in Figure 7.3, showing the beam irradiance, G_b , from the same day. Figure 7.2 shows the power output from the 20th August 2017. It was a cloudy day, with large fluctuations in the cloud cover. This can be seen in Figure 7.4, where large fluctuations in the beam irradiance can be observed. In Figure 7.1 and Figure 7.2 the measured power output is represented by the blue line, the predicted output without a_3 is represented by the orange line, and the predicted output including a_3 is represented by the yellow line.

From Figure 7.1, representing the sunny day, it can be seen that the measured power output and the predicted models are following the same pattern, even though the predicted power output is higher than the measured. There is a small deviation between the two predicted curves, showing the model including a_3 has a slightly better fit, but there seems to be no significant difference.

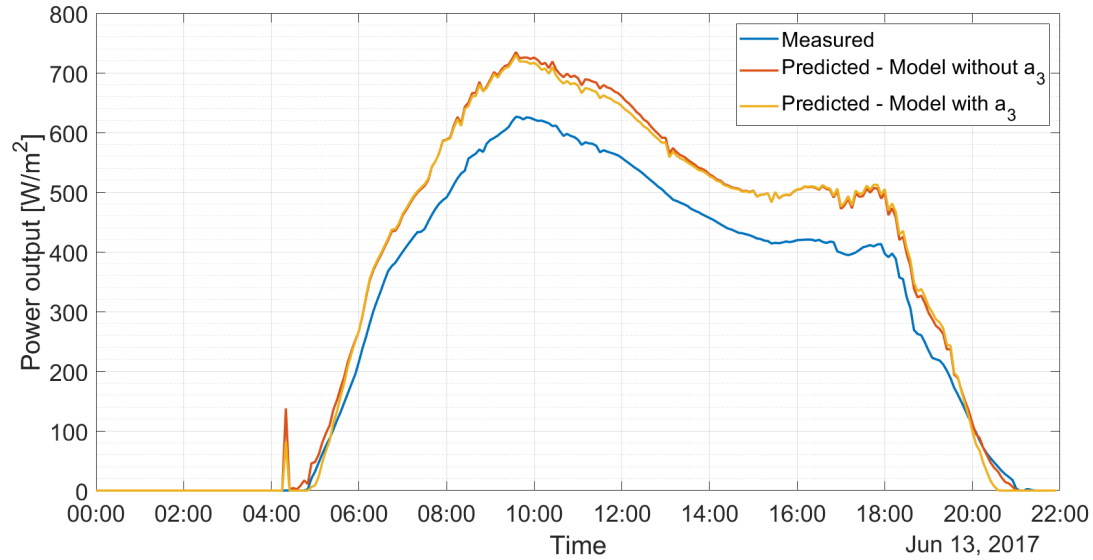


Figure 7.1: Useful power output in $\left[\frac{\text{W}}{\text{m}^2}\right]$ for the PTC field on a sunny day - the 13th of June 2017: Measured (blue curve), predicted with model without a_3 (orange curve), and predicted model with a_3 (yellow curve). The x-axis is showing the local time.

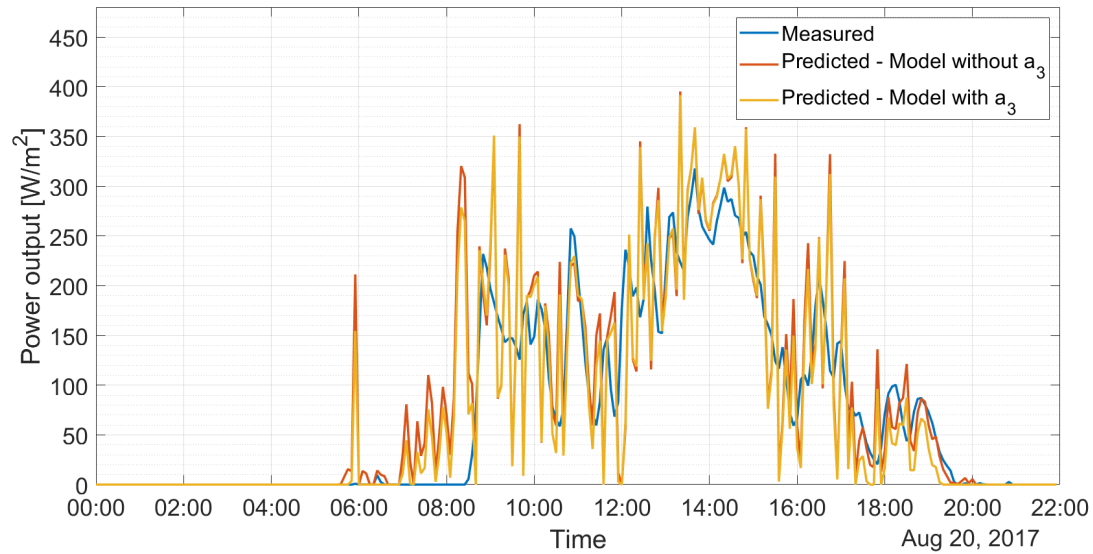


Figure 7.2: Useful power output in $\left[\frac{\text{W}}{\text{m}^2}\right]$ for the PTC field on a cloudy day - the 20th of August 2017: Measured (blue curve), predicted with model without a_3 (orange curve), and predicted model with a_3 (yellow curve). The x-axis shows the local time.

Figure 7.2, which shows the comparison on a cloudy day, does also show that the measured and predicted values are following the same pattern, but there is large fluctuations in the predicted power output. This is caused by a large fluctuation in the received radiation, due to changing weather condition between sun and cloud cover. This results in predicted power output which is both under and over estimated compared to the measured power output. Looking closely at the graph, it can be seen that the model including a_3 is slightly closer to the measured output.

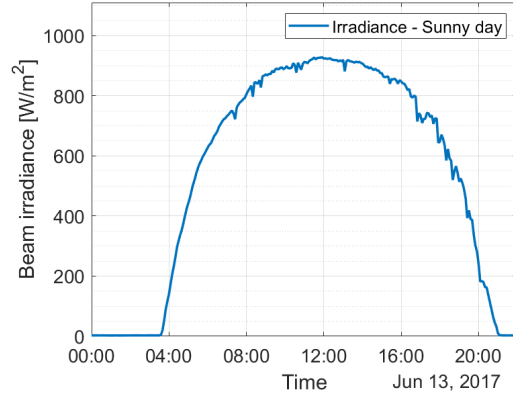


Figure 7.3: Beam irradiance in $\left[\frac{\text{W}}{\text{m}^2}\right]$ on a sunny day - the 13th of June 2017. The x-axis shows the local time.

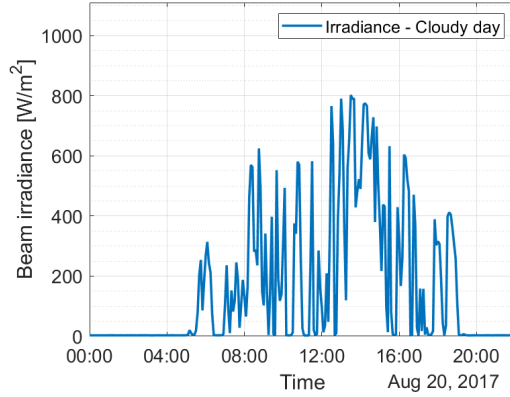


Figure 7.4: Beam irradiance in $\left[\frac{\text{W}}{\text{m}^2}\right]$ on a cloudy day - the 20th of August 2017. The x-axis is shows the local time.

For the cloudy day the measured useful energy output only for this day is $1.6 \frac{\text{kWh}}{\text{m}^2}$, the predicted output for the model without a_3 is $1.9 \frac{\text{kWh}}{\text{m}^2}$, and the predicted output for the model with a_3 is $1.7 \frac{\text{kWh}}{\text{m}^2}$. These results show, that even though the fluctuations seem large in the Figure 7.2 the total predicted energy output for the day is very close to the measured.

To get a better understanding of the comparison between the measured and predicted values, the useful energy output is found and compared as well. This will also verify if the model can be used for long term predictions. The energy output, E_{output} , is calculated as a total energy value in $\frac{\text{kWh}}{\text{m}^2}$ for each month. In Eq. 7.1 the calculation is shown.

$$E_{output} = \left(\frac{Q \cdot dt}{3600}\right) \cdot 10^{-3} \quad (7.1)$$

Q is the power output in $\frac{\text{W}}{\text{m}^2}$, and dt is the number of seconds between each data point.

Below in Table 7.1 the energy output is listed. In Figure 7.5 the output is shown in a bar chart, as a graphical representation as well. In the bar chart the measured useful energy output is represented by the blue bars, the predicted output for the model without a_3 is represented by the orange bars, and the predicted output for the model with a_3 is represented by the yellow bars.

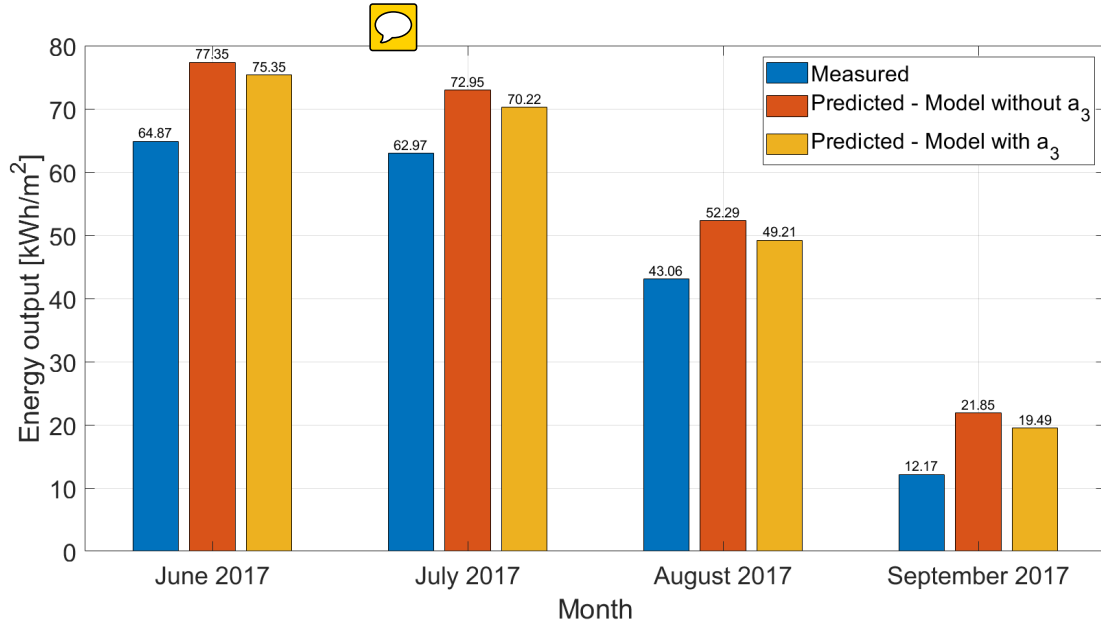


Figure 7.5: Bar chart showing the total useful energy output in $\left[\frac{\text{kWh}}{\text{m}^2}\right]$ for the PTC field for June, July, August, and September 2017: Measured (blue curve), predicted with model without a_3 (orange curve), and predicted model with a_3 (yellow curve).

Energy output in $\left[\frac{\text{kWh}}{\text{m}^2}\right]$			
Month	Measured	QDT model without a_3	QDT model with a_3
<i>June</i>	64.87	77.35	75.35
<i>July</i>	62.97	72.95	70.22
<i>August</i>	43.06	52.29	49.21
<i>September</i>	12.17	21.85	19.49

Table 7.1: The measured monthly energy output and predicted energy output for the QDT models without and with a_3 in $\left[\frac{\text{kWh}}{\text{m}^2}\right]$ for June, July, August and September 2017.

Looking at the difference in the monthly energy output between the two QDT models in Table 7.1 and Figure 7.5 a small difference can be seen as in Figure 7.1 and Figure 7.2 above. The difference is not significant, but though does the modified QDT model including a_3 give results closer to the measured energy output.

Further knowledge for the comparison can be gained from Table 7.2, which shows the percent relative error, relative error in [%], of the predicted energy output, in comparison to the measured energy output. The percent relative error, RE , is found as in Eq. 7.2 [32].

$$RE = \frac{|Q_{predicted} - Q_{measured}|}{Q_{measured}} \cdot 100 \quad (7.2)$$

Relative error for predicted power output in [%]		
Month	QDT model without a3	QDT model with a3
<i>June</i>	19	16
<i>July</i>	16	12
<i>August</i>	21	14
<i>September</i>	80	60

Table 7.2: The relative error in [%] for the predicted monthly energy output for the QDT models without and with a_3 compared to the measured monthly energy output for June, July, August and September 2017.

Looking at Table 7.2 showing the relative errors, it can be seen that there is a difference of 16-21% for the model without a_3 , and 12-16% for the model with a_3 for June, July and August. The relative error concludes that the modified QDT model including a_3 is giving better results. For September the relative error is very large, which was also seen in Table 7.1. This is due to an error in the code for the validation for that month, and should not be considered as the correct output of the model for September.

The values for the relative error can be compared to the values found in an earlier report (Mihalitsis, 2020 [3]), investigating the same collector field. The relative error was in the report found to be between 18-23% as seen below in Table 7.3.

Relative error in [%] found in earlier study (Mihalitsis, 2020 [3])	
Month	Relative error [%]
<i>June</i>	20
<i>July</i>	23
<i>August</i>	18
<i>September</i>	19

Table 7.3: Relative error in [%] for predicted power output found from earlier study (Mihalitsis, 2020 [3]).

Comparing this thesis to (Mihalitsis, 2020 [3]) an improvement has been done in this thesis, and especially for the model including a_3 , when looking on the relative error.

7.2 Lendemarke - Fresnel lens solar collector field

The validation of the Lendemarke field is done using the same data set as for the MLR. First a graphical comparison of the predicted and measured useful power output is performed. Below in Figure 7.6 the measured power output is shown by the blue curve, and the predicted power output from the QDT model in Eq. 5.9 is shown by the orange curve. In Figure 7.7 the beam irradiance for the same time period is shown.

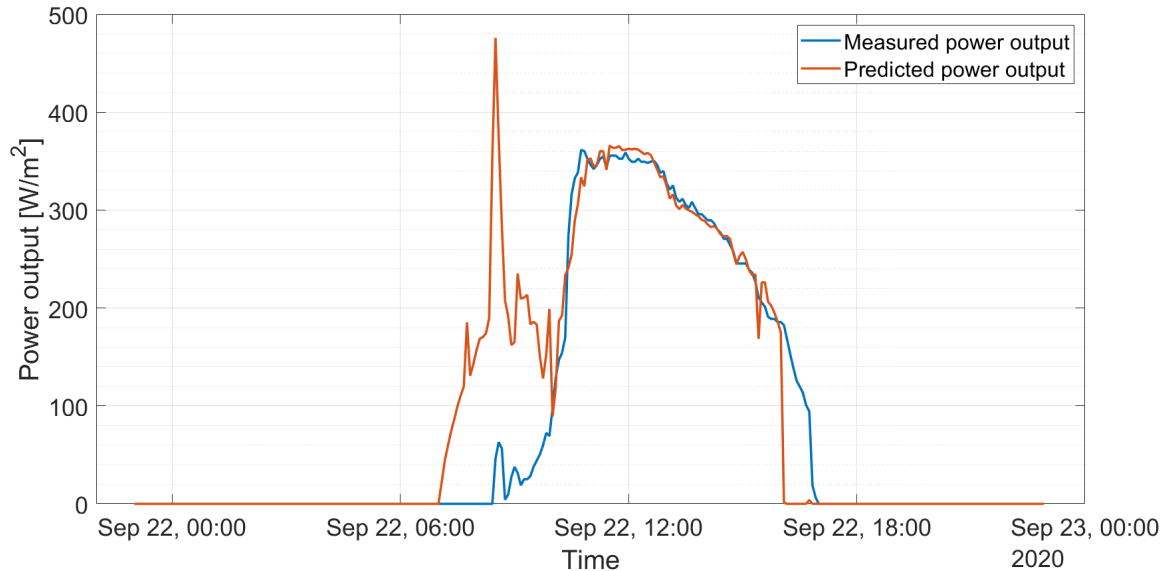


Figure 7.6: Useful power output in $\left[\frac{\text{W}}{\text{m}^2}\right]$ for the Fresnel lens collector field on the 22nd of September 2020: Measured (blue curve) and predicted (orange curve). The x-axis shows the local time.

From Figure 7.6 it is seen that the predicted power output is following the same pattern, as the curve for the measured power output, though there are a few peaks for the predicted output. From Figure 7.7 it can be seen, that the validation is done for a sunny day, and therefore there is no big fluctuations in the predicted power output.

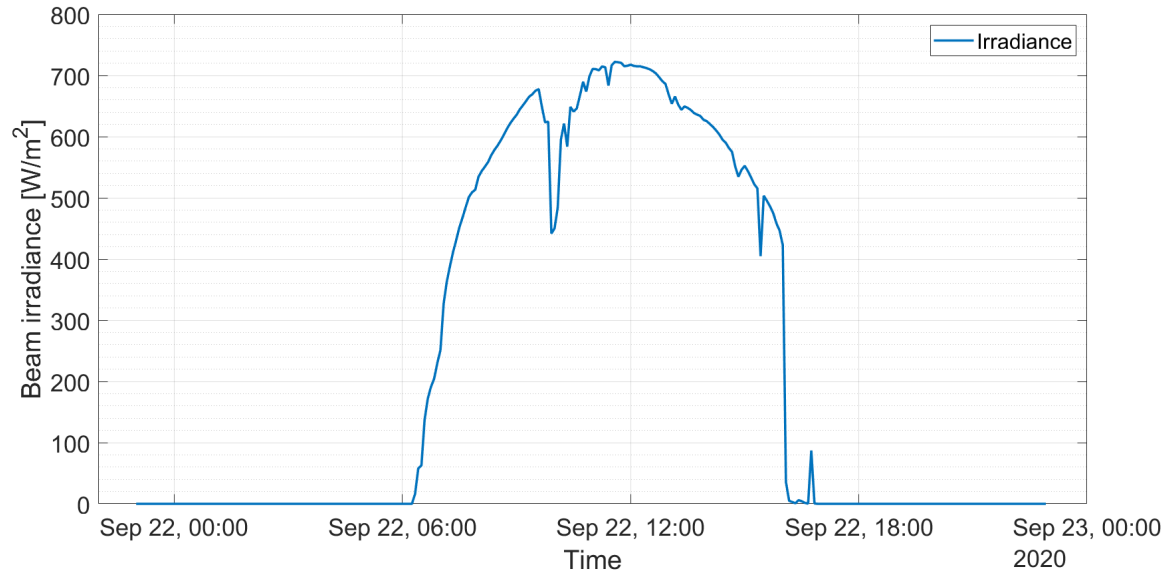


Figure 7.7: Beam irradiance in $\left[\frac{W}{m^2}\right]$ on the 22nd of September 2020. The x-axis shows the local time.

Below in Table 7.4 the measured and predicted useful energy can be seen. The energy output is given in $\frac{kWh}{m^2}$, and was found as shown in Eq. 7.1 above. In the table the relative error of the predicted output compared to the measured output is also shown. The relative error was found as shown in Eq. 7.2 above.

Output parameters for the Fresnel lens collector field		
Measured useful energy output $\left[\frac{kWh}{m^2}\right]$	Predicted useful energy output $\left[\frac{kWh}{m^2}\right]$	Relative error [%]
1.92	2.28	18.75

Table 7.4: Table showing the measured useful energy output in $\left[\frac{kWh}{m^2}\right]$, the predicted useful energy output in $\left[\frac{kWh}{m^2}\right]$, and the relative error in [%] for the Fresnel lens collector field on the 22th of September 2020.

As shown in Table 7.4 the measured useful energy output for the 22nd of September 2020 is 1.92 $\left[\frac{kWh}{m^2}\right]$, and the predicted output was 2.28 $\left[\frac{kWh}{m^2}\right]$, leading to an relative error of 18.75%. The relative error is high, and could be desired lower, despite this the graphical representation seen in Figure 7.6 shows that the curves are to some extend very similar.

Since only data for a sunny day is available, it can be difficult to validate the model for transient

weather conditions and longer term performance predictions. Even though, the model validation shows similar results to the validation of the PTC field, in terms of relative error. It could be expected that the model will perform as well on cloudy days, as on sunny days, and for longer term predictions.

Chapter 8

Discussion and future work

In this chapter possible reasons for the difference in the calculated and predicted useful output will be discussed. Future improvement of the model will also be discussed.

Discussion

The performance of the mathematical model for the PTC field and FLC field is in the same range. The relative error of the predicted useful energy output for the PTC field was found to be approximate 16-21% for the model without a_3 , and for the FLC field it was found to be approximate 19%. This error can indicate that the model can be used for both CSP fields, but that it should also be modified, so a lower relative error is obtained.

The mathematical model can be improved, and a way to do it, is to implement more terms related to the construction of the CSP fields. The collector fields are not always working under perfect ideal conditions, which means that multiple and naturally occurring factors will affect the useful outputs and the relative error. These factors might be possible to account for in a further mathematical model.

For both collector fields it could be seen in Figure 7.3 and Figure 7.6 that the predicted power output starts earlier in the morning than the measured power output. In the afternoon the predicted power output stopped earlier than the measured. In Table 8.1 the start and stop time in local time for the useful power output for the FLC field can be seen. This shows the large variation.

Time interval for power production for Fresnel lens collector field - September 22nd 2020		
	Measured	Predicted
Power output start [local time]	8:25	7:00
Power output stop [local time]	17:00	16:05

Table 8.1: Table showing the start and stop time [local time] of the power production for the Fresnel lens collector field in the 22nd of September 2020 for the measured output and predicted output.

When the solar radiation is received by the collectors in early morning, the first received energy will not be used for heating up the HTF. Instead the energy is used to heat up the receiver. This will also be the case, at any other time, where the receiver has cooled down, and then is exposed to radiation. At these times the radiation hitting the collector will not be used as useful output, even though the QDT model would expect it to be. This might cause a deviation between the predicted and measured useful output. To which extent is however unknown for now.

The predicted power production stops before the measured output. When the sun sets and the radiation on the collector is limited, the model will not predict any power output, but the HTF might still contain some residual heat, which can be measured. The predicted power output is dependent on the beam irradiance in the exact moment, which will result in a power output given as a snapshot, when using the investigated QDT model. This will mean, that if no irradiance is received by the collectors, the predicted useful power output will be zero.

The QDT model from ISO 9806:2017 [6] is described as a test method for a single collector. In this thesis the test method has been applied for an entire collector field. T_f in the QDT model is the average temperature between the inlet and outlet temperature as seen in Eq. 5.3. The inlet and outlet temperature of the collector are measured at the same time. With the short distance between the inlet and outlet this will not affect the output. When T_f is found for the collector field, the inlet and outlet temperature are also measured at the same time, but the distance between the inlet and outlet is much larger than for a single collector, since the distance now is for an entire field. The test conditions are dynamic, which means that large changes in the solar radiation can happen, and affect the outlet temperature in short time. This might cause an inconsistent error in the measured mean fluid temperature, which is not accounted for in the evaluated QDT model. This could affect the calculated predicted useful output.

For the FLC field, it might improve the model to include a shading coefficient in the QDT model. Even when the collectors are a 2-axis tracking collectors, the output can be affected by internal shading from other collectors in the field.

The addition of the term a_3 for the PTC field improved the model, leading to a relative error of 12-16%. This might reveal that the heat loss is more complex than expected. Further investigations need to be done.

The validation of the mathematical model without the a_3 term shows similarity for both CSP fields. It leads to the assumption that a common QDT model can be used for both CSP fields. Though,

should some changes be done, and further work with the model, should decrease the relative error.

Future work

Above in the discussion many factors, that perhaps influence the predicted useful output was presented. For future work some of these could be implemented in the QDT model, which might will improve the model.

When the constants were found for the QDT model, the heat loss coefficient a_2 was found to be positive. A first step for future work could be to investigate this further. Also the validation for the PTC field for September should be corrected. For the FLC field an implementation to the model could be to add a shading coefficient for 2-axis tracking collectors.

Next the implementation of the new a_3 -term should be investigated further. The results from the validation showed a promising improvement, but it should also be tested for the FLC, to substantiate the theory.

The effect of the start and stop time for the power production, as well as the time delay between T_{in} and T_{out} could be very interesting to investigate, to see if those cause any deviation in the useful output.

Chapter 9

Conclusion

In this thesis a general mathematical model for a parabolic trough collector field and Fresnel lens collector field based on quasi-dynamic testing has been developed. The model analysed the performance of the solar collector fields in-situ, using existing data from the collector fields.

For both collector fields the mathematical model was validated with data from the fields. The validation both showed the short term and long term performance of the collector fields. For the parabolic trough collector field, the validation was performed with transient weather data for multiple months, whereas data from a single day was used for the Fresnel lens collector field. The largest relative error of the predicted useful energy output compared to the measured useful energy output was found to be 21%. This is an improvement from earlier studies. For the parabolic trough collector the peak efficiency was found to be 59.98%. For the Fresnel lens collector it was found to be 61%.

The thermal performance of both collector field was found to be very similar. The peak efficiencies and the relative error for the predicted energy output were close.

A modified model including a new term a_3 was also developed and validated for the parabolic trough collector field. For the modified model the largest relative error was found to be 16%, and the peak efficiency of the collector was found to be 61.32%. These results are very promising and the addition of a_3 should be investigated further.

For the model development and validation a program was developed as the solving tool. MATLAB was used as the programming platform.

Improvement of the mathematical model could be done, to obtain a lower relative error for the useful predicted energy output. This could e.g. be done by removing the heat loss a_2 or integrate the delayed power production in morning and resident heat in the afternoon. Further, to improve the model for the Fresnel lens collector, a shading coefficient for 2-axis tracking collectors could be added.

The mission for this thesis was to give an accurate prediction of the thermal performance for two concentrating solar collector fields. This has been accomplished, but could still be improved.

The main vision for this project was to "ensure all energy production is sustainable". This is a change, that consist of many solutions combined together. One solution could and should be to use energy from the sun. From this thesis the potential for solar heating fields have been evaluated. In a world with desperate need for more clean energy, solar heating collector fields has huge potential, which should be investigated and developed even further.

Bibliography

- [1] *Aalborg CSP website - Brønderslev collector field*. URL: <https://www.aalborgcsp.dk/projekter/166-mwt-csp-solvarmeanlaeg-i-broenderslev-danmark/>. (Accessed: 19.07.2021).
- [2] Alejandro de la Vega Fernandez. “Analyses of Brønderslev solar energy plant by use of TRN-SYS”. In: (2017).
- [3] Alexis Mihalitsis. “Development and validation of a test method for parabolic trough solar collector fields in solar heating plants”. In: (2020).
- [4] C.B.Honsberg and S.G.Bowden. *Photovoltaics Education Website*. 2019. Chap. 2. URL: <https://www.pveducation.org/>.
- [5] Climate-KIC. *Heliac challenges everything we know about energy*. URL: <https://nordic.climate-kic.org/news/heliac-challenges-everything-we-know-about-energy/>. (Accessed: 19.07.2021).
- [6] Danish Standard Associations. “Solar energy - Solar thermal collectors - Test methods (ISO 9806:2017)”. In: (2017).
- [7] *Description of ScenoCalc (Solar Collector Energy Output Calculator), a program for calculation of annual solar collector energy output*. 2019. URL: <http://www.estif.org/solarkeymarknew/component/content/article/13-public-area/163-scenocalc>.
- [8] John A. Duffie and William A. Beckman. *Solar Enguneering of Thermal Processes*. John Wiley Sons, 2013. ISBN: 978-0-470-87366-3.
- [9] *EnergiWatch*. URL: <https://energiwatch.dk/Energinyt/Renewables/article11879308.ece>. (Accessed: 28.06.2021).
- [10] Stephan Fischer, Carsten Lampe Peter Kovacs, and Enric Mateu Serrats. *IEA-SHC TASK 43: SOLAR RATING AND CERTIFICATION PROCEDURES*. Solar heating and cooling program - International energy agency, 2013.
- [11] *Google Maps*. URL: <https://www.google.dk/maps>. (Accessed: 20.06.2021).
- [12] *Heliac website*. URL: <https://www.heliac.dk/faq/>. (Accessed: 28.06.2021).
- [13] *Insider news publication*. URL: <https://www.businessinsider.com/this-is-the-potential-of-solar-power-2015-9?r=US&IR=T>. (Accessed: 25.07.2021).
- [14] Adam R. Jensen. *Test of Heliac 3rd Gen. Solar Collector - Solar Collector Thermal Performance and Pressure Drop Test according to ISO 9806:2017*. 2020. ISBN: 87-7877-544-2.

BIBLIOGRAPHY

- [15] Adam R. Jensen. *Abstract - Thermal performance assessment of the world's first Fresnel lens solar collector field*.
- [16] Adam R. Jensen, Simon Furbo, and Bengt Perers. *Brønderslev Hybrid Solar Power Plant - Performance Analysis and Monitoring Report*. 2020.
- [17] Kyriacos Chimoni. "Mathematical modeling and simulation for thermal performance calculation of parabolic trough solar collectors". In: (2021).
- [18] Keith Lovegrove and John Pye. *Concentrating Solar Power Technology - Principles, Developments, and Applications*. Woodhead Publishing, 2012. Chap. 2 - Fundamental principles of concentrating solar power systems. ISBN: 9781845697693.
- [19] Keith Lovegrove and Wes Stein. *Concentrating Solar Power Technology - Principles, Developments, and Applications*. Woodhead Publishing, 2012. Chap. 1 - Introduction to concentrating solar power technology. ISBN: 9781845697693.
- [20] M. Eck, T. Hirsch, J. F. Feldhoff, D. Kretschmann, J. Dersch, A. Gavilan Morales, L. Gonzalez-Martinez, C. Bachelier, W. Platzer, K.-J. Riffelmann and M. Wagner. "Guidelines for CSP Yield Analysis - Optical Losses of Line Focusing Systems; Definitions; Sensitivity analysis and Modelling Approaches". In: *Energy Procedia* (2013).
- [21] Bengt Perers et al. *A CSP plant combined with biomass CHP using ORC-technology in Brønderslev Denmark*. 2016.
- [22] S. Fischer, W. Heidemann, H. Müller-Steinhagen, B. Perers, P. Bergquist, B. Hellström. "Collector test method under quasi-dynamic conditions according to the European Standard EN 12975-2". In: *Solar Energy* (2003).
- [23] D. Sakthivadivel et al. *Renewable-Energy-Driven Future*. 2021. Chap. 1 - Solar energy technologies: principles and applications. ISBN: 9780128205396.
- [24] *Solar Tracking*. URL: <http://www.solarpanelsplus.com/solar-tracking/>. (Accessed: 22.06.2021).
- [25] William B. Stine and Michael Geyer. *Power from the sun*. 2001. Chap. 4. URL: <https://www.powerfromthesun.net/Book/chapter04/chapter04.html>.
- [26] Sven Fahr, Daniel Tschopp, Jan Erik Nielsen, Korbinian Kramer, Philip Ohnewein. "Review of In Situ Test Methods for Solar Collectors and Solar Collector Arrays". In: (2020).
- [27] *The Global Goals for Sustainable Development*. URL: <https://www.globalgoals.org/7-affordable-and-clean-energy>. (Accessed: 19.07.2021).
- [28] *towardsdatascience.com*. URL: <https://towardsdatascience.com/multiple-linear-regression-for-manufacturing-analysis-c057d4af718b>. (Accessed: 25.07.2021).
- [29] Michael J. Wagner and Paul Gilman. *Technical Manual for the SAM Physical Trough Model*. NREL - National Renewable Energy Laboratory, 2011.
- [30] Weiqiang Kong, Simon Furbo and Bengt Perers. "Development and validation of an in situ solar collector field test method". In: (2019).
- [31] *www.e-education.psu.edu/*. URL: <https://www.e-education.psu.edu/eme811/node/676>. (Accessed: 25.07.2021).

BIBLIOGRAPHY

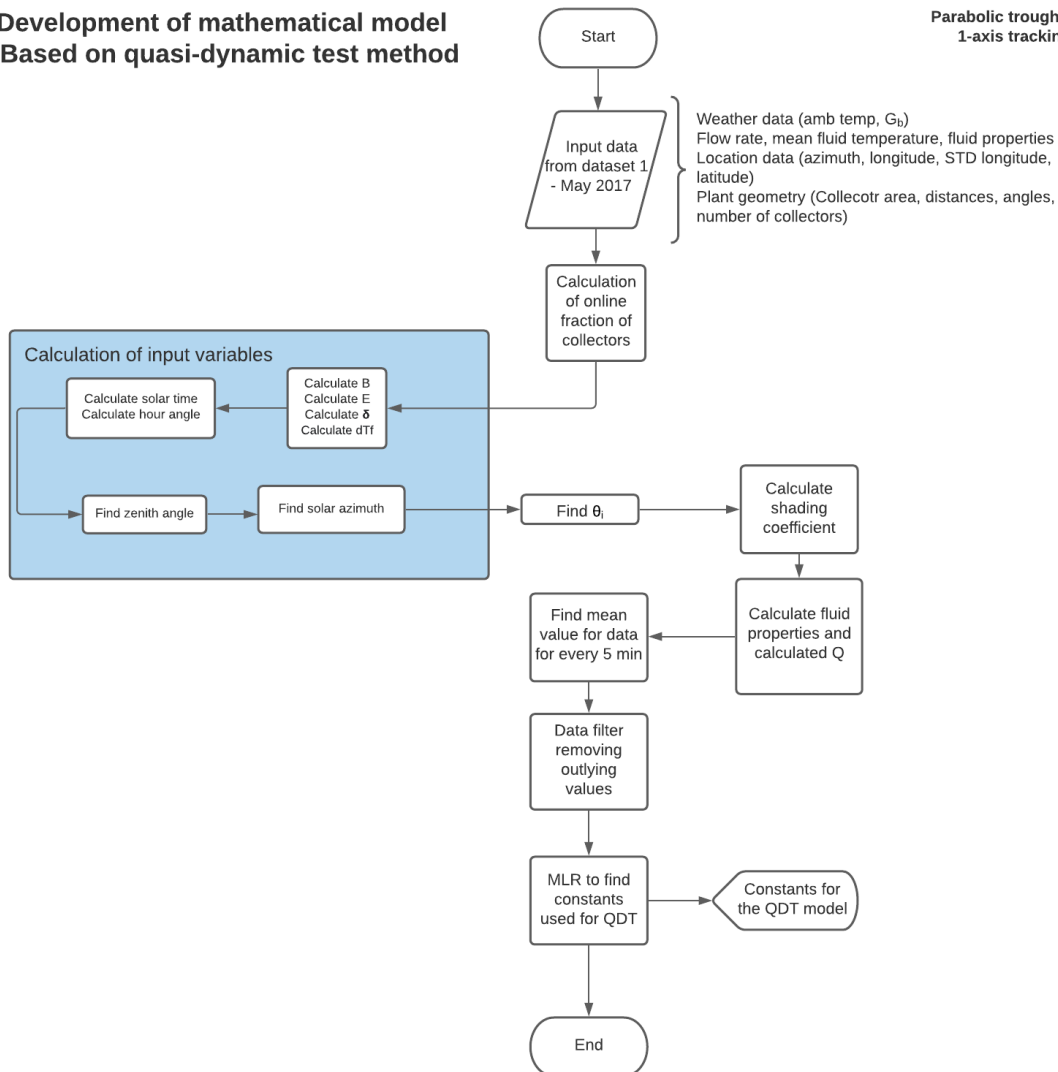
- [32] *www.onlinemathlearning.com*. URL: <https://www.onlinemathlearning.com/relative-error-formula.html>. (Accessed: 20.07.2021).
- [33] *www.renewableenergyhub.co.uk*. URL: <https://www.renewableenergyhub.co.uk/main/solar-thermal-information/the-different-types-of-solar-thermal-panel-collectors/>. (Accessed: 25.07.2021).
- [34] *www.solarreviews.com*. URL: <https://www.solarreviews.com/blog/what-are-the-most-efficient-solar-panels>. (Accessed: 25.07.2021).

Appendix A

Flowchart of the code written to find the constants in the QDT model for the parabolic trough collector field.

Development of mathematical model - Based on quasi-dynamic test method

Parabolic trough collector field - 1-axis tracking collectors



Appendix B

Flowchart of the code written to calculate the predicted useful power output for the parabolic trough collector field.

Validation of mathematical model - Finding useful power output

Parabolic trough collector field -
1-axis tracking collectors

